ADVANCED ENERGY MATERIALS
www.advenergymat.de

Locating Non-Radiative Recombination Losses and Understanding Their Impact on the Stability of Perovskite Solar Cells During Photo-Thermal Accelerated Ageing

Zijian Peng, Jonas Wortmann, Jisu Hong, Shuyu Zhou, Andreas J. Bornschlegl, Julian Haffner-Schirmer, Vincent M. Le Corre, Thomas Heumüller, Andres Osvet, Barry P. Rand, Larry Lüer,* and Christoph J. Brabec**

Commercialization of perovskite solar cells (PSCs) requires further breakthroughs in stability, but the complex degradation mechanisms and the interplay of the underlying stress factors complicate insight-driven improvement of long-term stability. This study establishes a quantitative link between potential degradation—specifically open-circuit voltage (V_{OC}) and quasi-Fermi level splitting (QFLS)—and the photo-thermal stability of PSCs. It is highlighted that an increase in non-radiative recombination losses induces the seemingly negligible decrease in V_{OC} and QFLS, though it causes a significant decrease in fill factor (FF) and/or short circuit current (J_{SC}) instead, leading to an overall performance decline. By combining non-destructive photoluminescence imaging and drift-diffusion simulations, it is revealed that during photo-thermal ageing, unstable low-dimensional passivation fails within tens of hours, generating bulk defects, while unstable hole-transport-layer contacts induce interface defects within hours. Building on these findings, a robust hole-transport-layer polymer interface is employed and enhanced perovskite crystal quality to suppress both interface and bulk defect generation during ageing, achieving a T_{80} lifetime exceeding 1000 h under accelerated ageing conditions (85 °C and two-sun illumination).

1. Introduction

Despite single-junction perovskite solar cells (PSCs) achieving a record efficiency of 26.95%, comparable to that of silicon cells, stability issues remain a significant barrier on the way toward a terawatt technology. Stability issues in PSCs arise from multiple factors, including moisture, oxygen, light, heat, bias, mechanical stress and the combinations thereof.[1–3]

The inherent instability of perovskites is largely attributed to their ionic nature which leads to substantial redox activity, mobilizing ionic species and triggering physical and chemical degradation. Ion migration can screen the electrical field, thus hindering charge extraction and promoting bulk recombination.[4–8] Additionally, under illumination, iodide oxidation creates iodide vacancies, interstitials, iodine, and triiodide (I_3^-).[9,10,11] The migration of iodide ions also may

Z. Peng, J. Wortmann, S. Zhou, A. J. Bornschlegl, J. Haffner-Schirmer, T. Heumüller, A. Osvet, L. Lüer, C. J. Brabec
Institute of Materials for Electronics and Energy Technology (i-MEET)
Friedrich-Alexander-Universität Erlangen-Nürnberg
91058 Erlangen, Germany
E-mail: zijian.peng@fau.de; larry.lueer@fau.de; christoph.brabec@fau.de

J. Wortmann, T. Heumüller, L. Lüer, C. J. Brabec
Helmholtz Institute Erlangen-Nürnberg for Renewable Energy (HIERN)
Forschungszentrum Jülich GmbH
91058 Erlangen, Germany

J. Hong, B. P. Rand
Department of Electrical and Computer Engineering
Princeton University
Princeton, NJ 08544, USA

The ORCID identification number(s) for the author(s) of this article can be found under https://doi.org/10.1002/aenm.202502787

DOI: 10.1002/aenm.202502787

V. M. L. Corre
Mads Clausen Institute
Center for Advanced Photovoltaics and Thin Film Energy Devices (SDUCAPE)
University of Southern Denmark
Sønderborg 6400, Denmark

B. P. Rand
Andlinger Center for Energy and the Environment
Princeton University
Princeton, NJ 08544, USA

Z. Peng, C. J. Brabec
Graduate School in Advanced Optical Technologies (SAOT)
91052 Erlangen, Germany

L. Lüer, C. J. Brabec
FAU Solar
Friedrich Alexander University Profile Center Solar
91052 Erlangen, Germany

cause the accumulation of interstitial iodides at interfaces.[12] These processes lead to deep-level defects, which significantly increase non-radiative recombination within both the bulk and interface regions.[13–15] Oxidized iodide migration into transport layers and further on toward electrodes induces additional redox reactions and corrosion that impede operation.[16–18] Additionally, the presence of cations such as methylammonium (MA) and formamidinium (FA) facilitate acid-base reactions with active hydroxyl groups at the surface of, e.g., metal oxides,[19,20] and subsequent reactions of deprotonated ammonium with Pb^{2+} or FA, which leads to metallic Pb and destabilizes the lead-iodine octahedral structure.[21–25] These degradation processes occur across multiple regions—bulk, interfaces, and electrodes—further complicating stability improvements.

Varying ageing conditions further challenge stability evaluation as different degradation mechanisms may dominate under different conditions and stages of the ageing process.[26,27] Standard protocols, such as those from the International Summit on Organic Photovoltaic Stability (ISOS),[28] have been developed to evaluate the stability of devices in a way that allows comparison between studies. Those based on photo-thermal accelerated ageing protocols are increasingly reporting T_{80} lifetimes exceeding 1000 h.[29–38] However, these protocols primarily evaluate device performance using standard current density–voltage (J–V) measurements, offering limited insights into the origin of residual degradation and their location at the bulk or at the interface. This limitation hinders to directly correlation of performance losses to specific degradation processes. For instance, during photo-thermal accelerated ageing, open-circuit voltage (V_{OC}) losses are often modest, while significant losses occur in short-circuit current density (J_{SC}) and fill factor (FF).[21,39–45] Yet, J–V curves alone cannot directly identify the root causes of these phenomena. While drift-diffusion simulations can provide a rough distinction of types of degradation (e.g., generation versus recombination losses),[46,47] an assignment of electrical performance loss to specific degradation mechanisms is rarely demonstrated[48], mainly due to a lack of characterization techniques that yield deep physical insight at acceptable experimental complexity.

In this work, drift-diffusion simulation is used to demonstrate the impact of various non-radiative recombination mechanisms on the device related J–V performance metrics (power conversion efficiency (PCE), V_{OC}, J_{SC}, and FF). We distinguish between nonradiative recombination mediated by deep traps in the bulk and by interface traps. The findings emphasize that deep bulk traps lead to a modest reduction in V_{OC}, while they come along with a significant decline in J_{SC}. This is in contrast to the impact of interface traps, where V_{OC} losses are modest, FF being affected most. By employing contactless photoluminescence (PL) techniques, non-radiative recombination was analyzed across different perovskite stacks during photo-thermal accelerated ageing. We observed that commonly used low-dimensional passivation and hole transport layers result in significant energy losses during the early stages of ageing. Once devices are fabricated with sufficiently stable interfacial contacts, our findings reveal that V_{OC} losses mainly stem from non-radiative recombination, primarily attributed to the bulk perovskite itself during the first tens of hours. This work provides a robust framework for correlating potential losses with device degradation, offering reasonable insights for improving PSC stability under operational conditions.

2. Experimental Section

Our work builds on recent achievements in PL imaging,[48–56] a widely used, non-contact, and non-destructive technique for characterizing solar cells. Photoexcitation generates excess charge carriers, altering the electrochemical potentials (quasi-Fermi levels) of electrons and holes. Quasi-Fermi level splitting (QFLS) refers to the energetic offset of the quasi-Fermi levels between electrons and holes in a non-equilibrium condition (Figure S1a, Supporting Information). In the ideal case, QFLS divided by elementary charge (QFLS/e) was the maximum value that the V_{OC} of a solar cell can reach. However, V_{OC} was often lower than the QFLS/e value due to energy level misalignment, Ohmic losses, and other reasons.[57] Defect-assisted recombination decreases the QFLS, as bulk defects and interfacial defects (with volume densities of $N_{t,bulk}$ and $N_{t,interface}$, respectively) can serve as recombination centers for separated electrons and holes. For intrinsic semiconductors, the charge carrier recombination kinetics can be described by

$$\frac{dn}{dt} = k_1\, n + k_2 n^2 \tag{1}$$

where n is the photogenerated charge carrier density, k_1 is the rate constant for defect-assisted 1st order recombination, k_2 is the rate constant for bimolecular radiative recombination. Note that we neglect Auger recombination owing to the low and medium carrier densities under solar illumination conditions. As k_1 is non-radiative and k_2 is radiative, and by assuming that all incident photons with an energy larger than the bandgap are absorbed by the perovskite layer and converted into free carriers, the photoluminescence quantum efficiency (PLQY) can be defined as,

$$PLQY = \frac{emitted\ photons}{absorbed\ photons} = \frac{k_2 n^2}{k_1 n + k_2 n^2} \tag{2}$$

in metal halide perovskites, k_1 is proportional to the defect density while k_2 is a property resulting from the band structure of the semiconductor and therefore assumed to be a constant for a given perovskite composition. A decrease in PL intensity under the same experimental condition can thus be assigned to an increase in k_1. The internal QFLS can be determined from the PLQY of the semiconductor:[58]

$$QFLS = QFLS_{rad} + kT\, ln\left(PLQY\right) \tag{3}$$

here $QFLS_{rad}$ is the radiative limit, representing the maximum QFLS without non-radiative loss. The QFLS difference between fresh and aged samples after degradation is

$$QFLS_{aged} - QFLS_{fresh} = \Delta QFLS = kT \ln\left(PLQY_{aged}/PLQY_{fresh}\right) \tag{4}$$

this logarithmic relationship indicates that small changes in QFLS correspond to significant differences in PLQY; for instance, a ten-fold reduction in PL intensity reflects only a 60 meV decrease in QFLS, as shown in Figure S1b (Supporting Information). Hence, PL/QFLS measurements offer a very sensitive method to gain detailed insights into recombination than V_{OC} measurements alone.

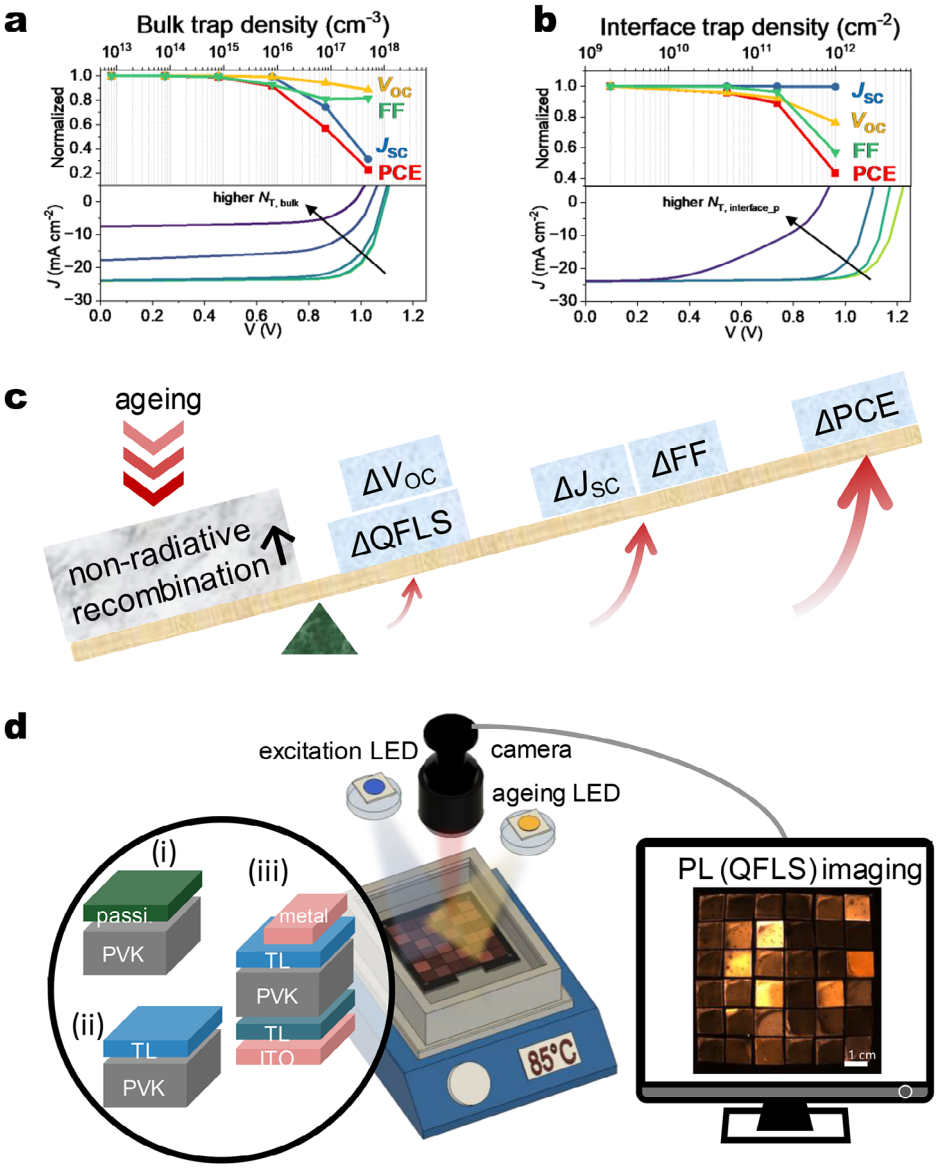

Figure 1. Impact of traps on device performance. Drift-diffusion simulations show the impact of the a) bulk, b) interface trap densities at HTL/PVK on the solar cell performance. In panel (a) the $N_{T, interface\_p}$ was kept constant (2e11 cm^{-2}), while in panel (b) the $N_{T, bulk}$ was kept constant (8e14 cm^{-3}). c) Schematic showing the correlation between device performance (V_{OC}, J_{SC}, FF, and PCE) and non-radiative recombination and QFLS. d) Schematic of photoluminescence (PL) imaging setup. Samples are placed inside a nitrogen-filled chamber on a hotplate. White LEDs (ageing LED) provide one-sun equivalent illumination for ageing tests. After white LED deactivation, 450 nm excitation LEDs with short-pass filters are used for PL excitation, while a camera with long-pass filters captures the PL image.

To quantify the effect of increasing defect-assisted non-radiative recombination on the device performance, drift-diffusion (DD) simulations were performed with the open-source tool SIMsalabim (v4.56)[59] varying the concentration of bulk defects ($N_{T, bulk}$), interfacial defects at hole transport layer (HTL)/PVK ($N_{T, interface\_p}$), interfacial defects at electron transport layer (ETL)/PVK ($N_{T, interface\_n}$), and the energy level of all traps (E_{trap}), as shown in **Figure** 1a,b and Figures S2 and S3 (Supporting Information). The device architecture ITO/ETL/perovskite/HTL/metal was used, and simulation parameters are listed in Table S1 (Supporting Information). As the bulk defect density increases, V_{OC} and FF decline rather slowly while a sharp drop in J_{SC} was observed at a critical defect density. This observation was attributed to the carrier recombination lifetime becoming significantly shorter than the extraction lifetime at higher defect density, making it difficult for carriers to be collected by the electrodes. The increase of interfacial defects at HTL/PVK had a larger impact on V_{OC} and FF, while the decrease of J_{SC} was not significant. The deepening of the energy level of all traps (away from the perovskite valence band) manifests in an ≈10% decrease in V_{OC} and FF. For bulk and interface defects, It was found that even a modest decrease in V_{OC} can correspond to substantial losses in FF and/or J_{SC}, which dominate performance degradation.

This was exactly the trend observed in various photo-thermal ageing tests,[21,39,40,43–45] as well as some outdoor tests.[41,42] In all these reports, V_{OC} tends to decrease modestly while the accompanying J_{SC} and FF losses dominate performance degradation. It was highlighted that what appears to be a negligible decrease in V_{OC} instead reflects an increase in the first order non-radiative recombination (Figure 1c), which was associated with significant J_{SC} and FF losses. Thus, the stability of perovskite materials and devices can be much more effectively screened by simply measuring the change in PL intensity and using the QFLS value as a critical indicator, which is representative for the changes in non-radiative recombination.

Our DD simulations provide plausible explanations for the observed trends by isolating the intrinsic impact of non-radiative recombination losses across stacks under controlled conditions. While factors like band offsets and layers' mobilities were not varied and could influence quantitative outcomes,[46,48,60] our concise approach establishes a benchmark for comparing relative performance degradation, enabling the efficient diagnosis of defect impacts within reasonable parameter ranges.

Various device were prepared structures to isolate the effects of charge extraction layers on non-radiative recombination. These included: i) perovskite bulk layer with or without surface passivation; ii) perovskite bulk layer with a single-side transport layer; and iii) stacks with double-side transport layers and/or electrodes (Figure 1d). Unencapsulated samples were placed in a nitrogen-filled chamber and exposed to accelerated ageing conditions (85 °C, one-sun illumination). For our imaging setup, PL was captured at different time intervals, with excitation provided by 450 nm LEDs and detection by a camera equipped with long-pass filters. Equation (3) can be rearranged as

$$QFLS_{sample} = QFLS_{rad} + kT\ ln\left(\frac{Red_{sample}}{Red_{ref}} \times PLQY_{ref}\right) \quad (5)$$

where $PLQY_{ref}$ is the PLQY of a reference (perovskite film without surface passivation), Red_{sample} and Red_{ref} are the number of counts recorded by the red channel of the camera. By obtaining the $PLQY_{ref}$ value with an integrating sphere and the Red_{ref} and Red_{sample} intensity values with our imaging setup, the $QFLS_{sample}$ of the sample can be calculated (Figure S4, Supporting Information). To reduce the influence of mobile ions and light-soaking effect on the QFLS measurement,[57,61,62] samples are preconditioned under light-soaking for at least 30 s before PL imaging, ensuring quasi-steady-state results. The QFLS values derived from this PL mapping are based on the average PL intensity over a defined area, in contrast to conventional steady-state PL, which measures smaller, localized regions. This approach not only provides statistically more robust results but also allows for the assessment of film homogeneity.

2.1. Non-Radiative Recombination Losses with Low-Dimensional Passivators

First, we investigated the passivation and stabilization effect of various low-dimensional perovskites (molecular structures shown in Figure S5, Supporting Information) under photo-thermal conditions (85 °C and one-sun, namely ISOS-L-2). The PL images were recorded at 0, 1, 4, 20, 100, and 300 h (**Figure 2a**). The corresponding trends in QFLS are shown in Figure 2b,c and Figure S6 (Supporting Information). Initially (before 0 h), as the temperature increases from 25 to 85 °C, QFLS decreases by ≈70 meV due to enhanced black body radiation that actually reduces $QFLS_{rad}$.

For the unpassivated sample (control), QFLS dropped continuously from 1.08 to 1.01 eV during the first 20 h, followed by a plateau extending up to 300 h. This indicates a rapid increase in non-radiative recombination early in the degradation process, which levels off after 20 h. In contrast, certain 2D-passivated samples (e.g.,Phenethylammonium iodide (PEAI) and n-Octylammonium iodide (OAI) as shown in Figure 2) exhibited a temporary rise in QFLS during the first hour, due to the diffusion of the ligand into the perovskite bulk, where the defect density is reduced, consistent with other studies.[63–66] Other passivators (e.g., n-Butylammonium iodide (BAI) and Guanidinium iodide (GuaI) in Figure S6a, Supporting Information) showed immediate QFLS decay during the first hour, suggesting different diffusion kinetics or passivation mechanisms.[67,68] However, after 20 h, QFLS of all passivated samples decreased to a level similar to that of the control group (≈1.02 eV), indicating that the passivation effect diminishes after extended ageing. The instability of 2D perovskite layers under photo-thermal ageing conditions was reported in our recent work.[45] The 2D decomposition was assigned to the deprotonation of the ammonium group of 2D ligand either followed by a reaction with a lead-iodine octahedron,[23,25] or followed by a nucleophilic reaction with another organic cation (e.g., FA^+),[21,69] which disassembles the 2D perovskite structure and renders them ineffective in the long term. Besides, the QFLS, bandgap, and Urbach energy trends (Figures S7–S10, Supporting Information) in passivated films under light-only or heat-only ageing condition differ greatly from those observed under combined light-heat ageing, indicating distinct ageing mechanisms in varying environments.

Devices fabricated from low-dimensional passivated films exhibited two key characteristics during photothermal ageing (Figure S11, Supporting Information): comparatively larger relative losses in V_{OC} than non-passivated control, and a dominant decline in J_{SC} that primarily drives the reduction in PCE for these passivated devices. Based on the above observations, a significant fraction of the 2D ligand is proposed to diffuse into the 3D bulk within the first few tens of hours, subsequently reacting with Pb-iodine octahedron to form metallic Pb defects during prolonged ageing.[23,25] These defects in bulk act as recombination centers, causing a modest reduction in V_{OC} but a significant decrease in J_{SC}, which aligns with the scenario modeled in our DD simulations (Figure 1a) where increasing bulk trap density produce comparable effects.

2.2. Non-Radiative Recombination Losses with Different Transport Layers

In addition, the photo-thermal stability of perovskite layers with various transport layers was investigated. Given that the redox potential of iodine ($I/I^- \approx -5.3$ eV) is close to the highest occupied molecular orbital (HOMO) of many HTLs and iodine-induced

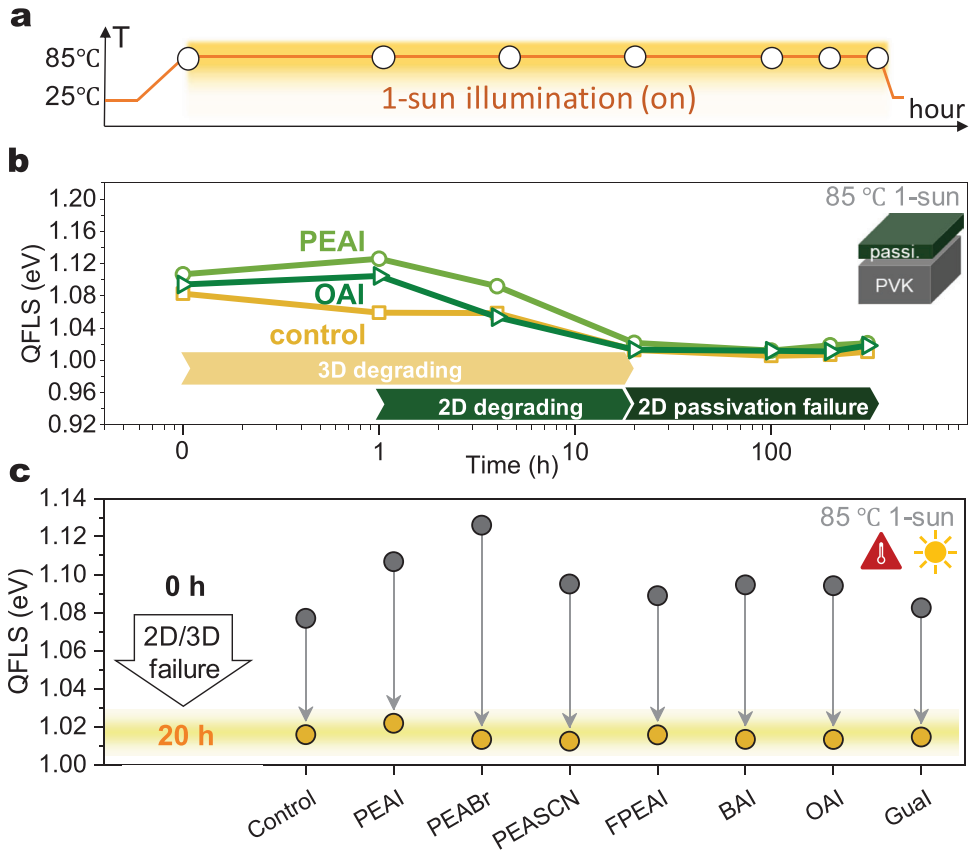

Figure 2. Non-radiative losses of perovskite films with low-dimensional passivators. a) Temperature profile during the ageing test. b) QFLS versus time. Before 0 h was the heat up region, from room temperature to 85 °C. Each data point is the average value of three samples. c) Changes in QFLS value of different passivated perovskite films before and after ageing under 85 °C and one-sun illumination for 20 h.

redox reactions during iodide migration greatly affect device stability, attention is focused on the stabilizing effect of HTLs (molecular structures shown in Figure S12, Supporting Information).

In **Figure** 3a, the QFLS of the glass/perovskite sample (glass/PVK) shows a rapid decline until it levels off, consistent with the above observations (Figure 2). Poly-[bis-(4-phenyl-2,4,6-trimethylphenyl)-amin] (PTAA) exhibits a similar trend but suffers more severe QFLS losses during the first hour of ageing (Figure 3a,c; Figure S14, Supporting Information). This degradation was typically discussed in terms of the diffusion of iodide and oxidized iodide species from the perovskite into the HTL. The diffusion of iodide species increases the iodide vacancy and interstitial concentrations in the bulk, enhancing non-radiative recombination.[12] Additionally, the accumulation of oxidized iodide species inside the HTL can lead to an oxidation of the HTL itself, increasing interfacial polaron concentration and exacerbating interfacial non-radiative recombination.[18] Doped PTAA (dopant: tris(pentafluorophenyl)borane (BCF)) and doped spiro-OMeTAD (2,2′,7,7′-Tetrakis[N,N-di(4-methoxyphenyl)amino]-9,9′-spirobifluorene) (dopant: lithium bis(trifluoromethanesulfonyl)imide (LiTFSI)) experience even larger QFLS losses (Figure 3e; Figure S13, Supporting Information), probably due to dopant diffusion into the perovskite layer, where they can act as non-radiative recombination centers.[70]

Previous studies have reported that organic materials with deeper HOMO levels can suppress halide diffusion from the perovskite into the HTL.[18] This was consistent with our findings. HTL samples with deeper HOMO levels, such as Poly[2,2′“”“-bis[[(2-butyloctyl)oxy]carbonyl][2,2′:5′,2′”:5′“,2′”“-quaterthiophene] -5,5′”“-diyl] (PDCBT), (poly(4,8-bis(5-chlorothiophen-2-yl)benzo[1,2-b:3,4-b”]-bis-thiophene) (PM7), and Poly[(2,6-(4,8-bis(5-(2-ethylhexyl)-4-chlorothiophen-2-yl)-benzo[1,2-b:4,5-b“]dithiophene))-alt-5,5′-(5,8-bis(4-(2-butyloctyl)thiophen-2-yl)dithieno[3′,2′:3,4;2′”,3′′:5,6]benzo[1,2-c][1,2,5]thiadiazole)] (D18-Cl), clearly exhibit smaller QFLS losses (Figure 3e). Notably, PDCBT maintains stable QFLS values throughout the ageing process (Figure 3a,c). To investigate the ability of polymers to block iodide species, iodine diffusion was monitored using an Ag:I_2 corrosion test, where conductance changes due to Ag electrode corrosion by I_2 indicate the extent of iodine diffusion through the polymers.[71,72] Figure S16 (Supporting Information) demonstrates that PDCBT effectively inhibits iodine diffusion, hence reducing iodine loss from the perovskite and stabilizing QFLS values. Lateral conductivity tracking experiments (Figure S17, Supporting Information) further confirm that PDCBT, PM7, and D18-Cl promote a more stable electrical contact interface. The deeper HOMO of CuSCN improves band alignment with perovskite, reducing the QFLS loss. However, CuSCN reacts readily with iodine,[73] accelerating the iodide loss from perovskite,

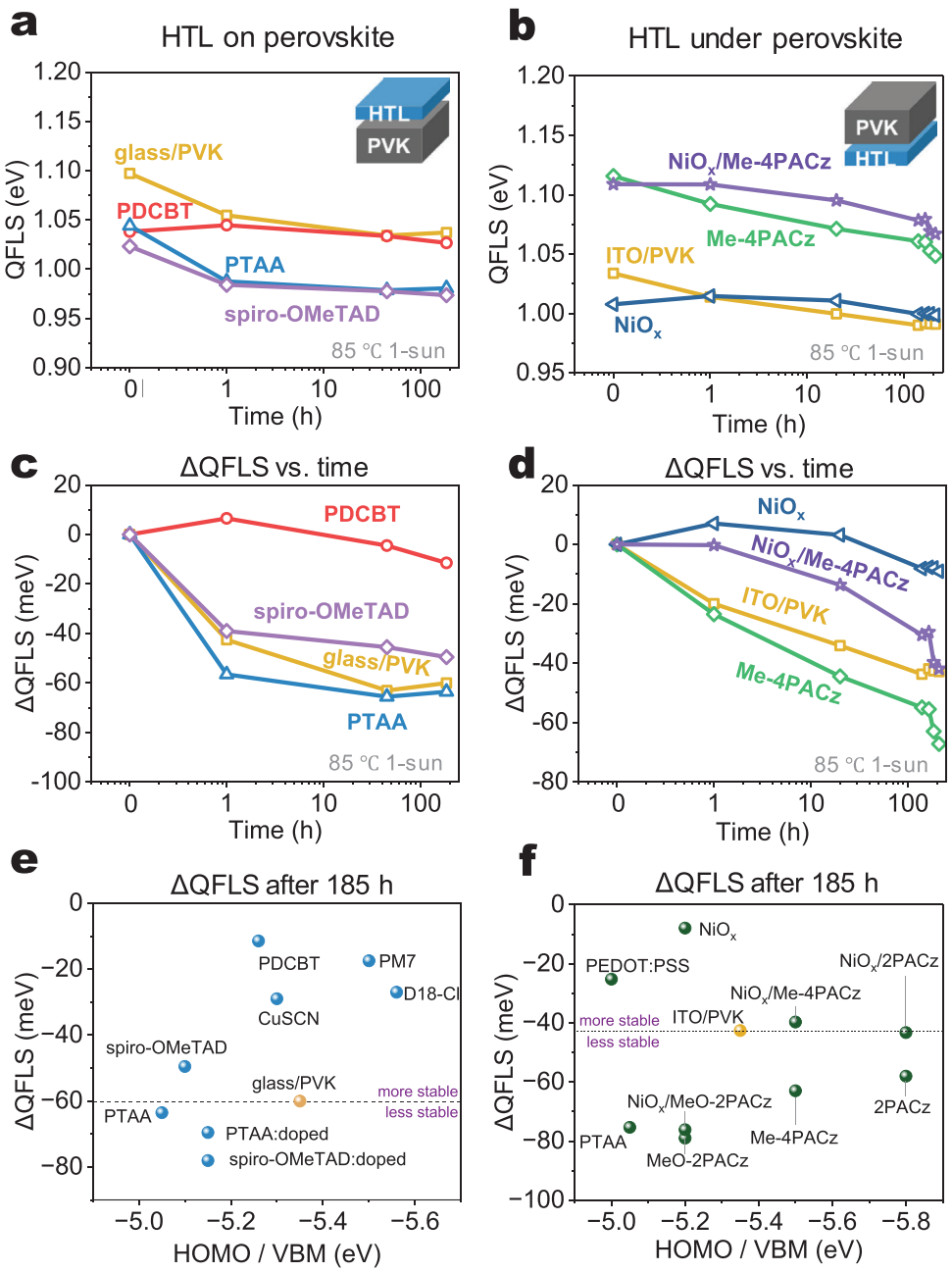

Figure 3. Non-radiative losses with different hole transport layers. a,b) QFLS value and c,d) change of QFLS as a function of time during photo-thermal ageing. e,f) QFLS changes of films (before and after ageing, $\Delta QFLS = QFLS_{185h,\ 85°C} - QFLS_{0h,\ 85°C}$) dependent on HOMO (or valence band maximum (VBM)) value of hole transport layers. HOMO/VBM values are based on literature.[40,82,85–91]

damaging perovskite structure and dedoping CuSCN itself, thereby exacerbating electrical contact (Figure S17, Supporting Information).

Overall, QFLS changes induced by the HTL on top of perovskite primarily occur during the initial hours of ageing, with subsequent changes driven by losses in the perovskite layer. This early QFLS "burn-in" losses can be largely mitigated by employing suitable hole transport layers (e.g., PDCBT, deeper HOMO and less reactive material) that effectively impede iodine diffusion. Further device ageing experiments (Figure S18, Supporting Information) reveal that PDCBT significantly mitigates the burn-in losses of FF compared to PM7 and D18-Cl as contacts, indicating suppressed formation of interface defects during degradation, as suggested by the DD simulations (Figure 1b).

The QFLS over time for HTL/PVK stacks (HTL beneath perovskite) was then assessed, as shown in Figure 3b,d,f and Figure S15 (Supporting Information). Images of these films before and after ageing are shown in Figure S22 (Supporting Information). While the NiO_x/PVK interface demonstrated a lower initial QFLS values, it shows a stable QFLS trend during ageing. The

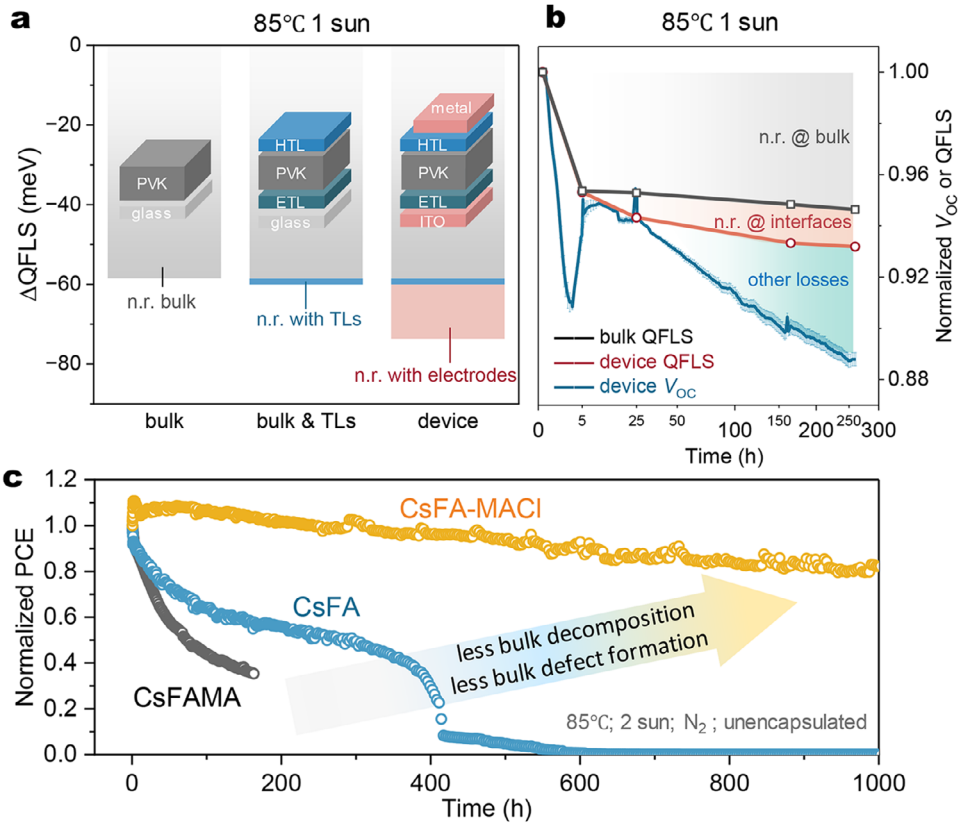

Figure 4. Non-radiative losses of full devices. a) QFLS changes in different stacks before and after ageing at 85 °C and one-sun illumination ($\Delta QFLS = QFLS_{260h,\ 85°C} - QFLS_{0h,\ 85°C}$). Bulk recombination dominates non-radiative losses in the full device. Here, the bottom TLs are SnO_2/PCBM, and the top TLs are PDCBT/PTAA: BCF.[40] b) Normalized V_{OC} and QFLS over time at 85 °C and one-sun. Abbreviation "n.r.@bulk" means non-radiative losses at bulk, and "n.r.@interfaces" means non-radiative losses at interfaces. c) Normalized PCE of devices with different components (CsFAMA, CsFA and CsFA-MACl) under 85 °C and two-sun illumination. The device architecture is ITO/SnO_2/PCBM/perovskite/PDCBT/PTAA: BCF/Au.

self-assembled monolayers (SAM)-based HTL, on the other hand, exhibits a continuous QFLS decrease during ageing, with a faster decay trend at the prolonged region (>100 h). This is attributed to the inherent chemical instability of SAM materials and interfacial instability. Conventional SAMs undergo desorption due to weak phosphate group and substrate's —OH bonding,[74–77] degrade under light/thermal stress,[78,79] and exhibit poor adhesion SAM/PVK, leading to voids formation[80] all of which deteriorate the passivation effect and exacerbate non-radiative recombination. Rational SAM molecular design and deposition optimization were needed to stabilize the SAM/PVK interface. The greater QFLS losses observed in MeO-2PACz-based samples compared to those with 2PACz or Me-4PACz probably result from its relatively inferior hole extraction capability[81] where accumulated holes at the interface promote ion migration[82] and accelerate iodide oxidation.[83,84] Notably, while deeper HOMO levels in top-HTL structures (perovskite/HTL) suppress iodide migration into the HTL and reduce QFLS losses (Figure 3e), this trend is absent in bottom-HTL structures (HTL/perovskite, Figure 3f). Here, iodine species primarily escape through the exposed perovskite surface rather than the HTL interface (Figure S19, Supporting Information). Materials like Poly(3,4-ethylenedioxythiophene) polystyrene sulfonate (PEDOT:PSS) and NiO_x exhibit minimal QFLS degradation – likely due to their ability to mitigate recombination center formation at both perovskite's bulk and their interface under photothermal stress, despite their shallow HOMO levels.

2.3. Non-Radiative Recombination Losses of Full Cells

To further investigate energy losses at the device level, we compare the QFLS variation across different stacks. Samples based on perovskite/ETL or ETL/perovskite structures exhibited greater QFLS losses upon ageing compared to perovskite-only samples (Figures S20,S21, and S23, Supporting Information), possibly a consequence of electron extraction, leaving excess holes in the perovskite which could lead to oxidative processes and perovskite degradation.[84,92] The HTL/perovskite/ETL stack reduces this excess of electrons or holes, and its QFLS loss was comparable to glass/perovskite alone. Interestingly, despite the continued addition of electrode layers (addition of Au electrodes and ITO electrodes), the QFLS loss of the stack remains comparable to that of the glass/perovskite (**Figure 4a**). It suggests that bulk recombination remains the primary source of non-radiative losses, provided sufficiently stable transport layers are deployed.

Figure 4b shows the change of normalized V_{OC} and QFLS at 85 °C under one-sun degradation. The blue curve represents the

normalized V_{OC} of the device, while the red and black curves show QFLS values from the PL imaging of the full device and perovskite film, respectively. During the first 5 h, normalized V_{OC} dropped rapidly to 91% and then rebounded to 94%, probably due to the effect of electrode depolarization.[93,94] Most non-radiative losses occur at the early stages (<25 h), driven primarily by perovskite degradation. As ageing progressed, the gap between device QFLS (red) and V_{OC} (blue) widened, suggesting additional "other losses" comparable with non-radiative recombination. These could include energy level misalignment due to de-doping of the transport layers and ion-induced field screening.[57,95]

After knowing that the main early degradation factor was the perovskite material itself, we optimized the active layer by replacing the CsFAMA ($Cs_{0.05}FA_{0.85}MA_{0.1}PbBr_{0.25}I_{2.75}$) composition with MA-free CsFA ($Cs_{0.15}FA_{0.85}PbBr_{0.25}I_{2.75}$). The elimination of the volatile and thermally unstable MA component was expected to suppress the formation of vacancy defects under thermal stress, as MA decomposition accelerates defect generation at elevated temperatures.[96,97] To ensure a highly qualitative crystalline perovskite layer, MACl was added into the precursor ink. The MACl additive influences primarily the early stages of film formation and mostly evaporates during annealing.[98–100] The residual Cl could enhance the activation energy for the migration of iodine ions and increase the formation energy of iodine vacancies by compressing the lattice.[101,102] Their *J*–*V* characteristics are shown in Figures S24 and S25 (Supporting Information). The above modification transferred into a remarkable stability improvement: a T_{80} lifetime exceeding 1000 h under 85 °C and two suns was observed (Figure 4c; Figures S27 and S28, Supporting Information), which was ≈30 times better than the MA-free CsFA device (T_{80} ~ 30 h), and 50 times better than the CsFAMA device (T_{80} ~ 18 h). The use of two suns intensity accelerates degradation processes, providing a strict and time-efficient method to evaluate long-term stability under realistic operational stresses, thereby enhancing the relevance of these results for practical applications. The activation energy for mobile ion migration in $FA_xMA_{1-x}PbI_3$ increases with higher FA content, explaining the enhanced stability of MA-free active layers.[103–105] Accompanying XRD analysis confirmed better crystal quality and a reduction in bulk defects, as evidenced by the stronger perovskite (100) diffraction peak and the weaker metallic lead (Pb^0) diffraction peak (Figure S29, Supporting Information). The more stable V_{OC} trend and stronger FF and J_{SC} retention (Figure S26, Supporting Information) suggest the suppressed formation of bulk defects during degradation, which is consistent with the mechanism proposed by the DD simulations (Figure 1a). It highlights the importance of optimizing perovskite composition and crystal quality to minimize bulk defect formation during photo-thermal ageing.

3. Conclusion

This study establishes a clear link between QFLS/V_{OC} degradation, and the stability of perovskite solar cells. By investigating non-radiative recombination losses before and after ageing in different perovskite stacks, we identified the key factors limiting photo-thermal stability. Unstable low-dimensional passivation materials and PVK/HTL interfaces generate bulk and interface defects during the early stages of ageing, respectively, causing modest V_{OC} decreases but resulting in significant J_{SC} and FF losses. Even with a robust contact interface, bulk defect formation within the perovskite itself persists during ageing, predominantly driving the initial V_{OC} and PCE decline. Optimizing perovskite composition and improving crystal quality can suppress defect formation, leading to a 50-fold improvement in photo-thermal stability. Importantly, this study demonstrates that full devices are not required for optimizing perovskite stability. Half-cells or electrode-free structures are sufficient for meaningful analysis, enabling non-contact degradation measurements and facilitating high-throughput screening of material recipes. While this work offers a rapid and effective approach to pinpointing the primary sources of performance degradation from a perspective of non-radiative recombination, achieving ultra-stable PSCs requires complementary strategies—discovery of robust transport layers with stable electrical properties against iodide/iodine diffusion. Such multi-dimensional approaches will be the key to overcome the multifaceted stability challenges in PSCs.

Supporting Information

Supporting Information is available from the Wiley Online Library or from the author.

Acknowledgements

C.J.B. gratefully acknowledges the financial support through the Bavarian Initiative "Solar Technologies go Hybrid" (SolTech), the DFG-SFB953 (project no. 182849149), DFG-GRK2495 (ITRG2495), and DFG-INST 90/917-1 FUGG. C.J.B, L.L. and A.J.B thank the Deutsche Forschungsgemeinschaft (DFG) for financial support from the project BR-4031/22-1. Z.P. and S.Z. acknowledge the financial support from China Scholarship Council. Z.P. acknowledges funding of the Erlangen Graduate School in Advanced Optical Technologies (SAOT) by the Bavarian State Ministry for Science and Art. J.H. and B.P.R. acknowledge support for this work by the United States Department of Energy's Office of Energy Efficiency and Renewable Energy (EERE) under their Solar Energy Technology Office (SETO) Award Number DE-EE0010503.

Conflict of Interest

The authors declare no conflict of interest.

Author Contributions

Z.P., L.L., and C.J.B. conceived the idea. L.L. and C.J.B. supervised the project. Z.P. designed the experiments and conducted the photoluminescence imaging measurements. Z.P. and V.M.L.C. performed the drift-diffusion simulations. Z.P., J.W., A.J.B., J.H.-S., and A.O. built the photoluminescence imaging setup. J.H. and B.P.R. carried out the iodine diffusion experiments. Z.P. and T.H. conducted the long-term stability tests. S.Z., A.J.B., J.W., J.H., and B.P.R. contributed to the interpretation and analysis of the results.

Data Availability Statement

The data that support the findings of this study are available from the corresponding author upon reasonable request.;

Keywords

2D/3D, accelerated ageing, degradation, drift-diffusion simulation, interfaces, perovskite, PL mapping, SAM, stability, transport layers

Received: May 21, 2025
Revised: June 30, 2025
Published online: July 10, 2025

[1] H. W. Zhu, S. Teale, M. N. Lintangpradipto, S. Mahesh, B. Chen, M. D. McGehee, E. H. Sargent, O. M. Bakr, *Nat. Rev. Mater.* **2023**, *8*, 569.
[2] Z. H. Dai, N. P. Padture, *Nat. Energy* **2023**, *8*, 1319.
[3] X. Liu, D. Luo, Z. H. Lu, J. S. Yun, M. Saliba, S. I. Seok, W. Zhang, *Nat. Rev. Chem.* **2023**, *7*, 462.
[4] W. Tress, N. Marinova, T. Moehl, S. M. Zakeeruddin, M. K. Nazeeruddin, M. Grätzel, *Energy Environ. Sci.* **2015**, *8*, 995.
[5] C. Eames, J. M. Frost, P. R. Barnes, B. C. O'Regan, A. Walsh, M. S. Islam, *Nat. Commun.* **2015**, *6*, 7497.
[6] J. Thiesbrummel, S. H. Shah, E. Gutierrez-Partida, F. S. Zu, F. Pena-Camargo, S. Zeiske, J. Diekmann, F. Y. Ye, K. P. Peters, K. O. Brinkmann, P. Caprioglio, A. Dasgupta, S. Seo, F. A. Adeleye, J. Warby, Q. Jeangros, F. L. Lang, S. Zhang, S. Albrecht, T. Riedl, A. Armin, D. Neher, N. Koch, Y. Z. Wu, V. M. Le Corre, H. Snaith, M. Stolterfoht, *Nat. Energy* **2024**, *9*, 664.
[7] V. M. Le Corre, J. Diekmann, F. Peña-Camargo, J. Thiesbrummel, N. Tokmoldin, E. Gutierrez-Partida, K. P. Peters, L. Perdigón-Toro, M. H. Futscher, F. Lang, J. Warby, H. J. Snaith, D. Neher, M. Stolterfoht, *Sol. RRL* **2022**, *6*, 2100772.
[8] I. M. Hermes, Y. Hou, V. W. Bergmann, C. J. Brabec, S. A. L. Weber, *J. Phys. Chem. Lett.* **2018**, *9*, 6249.
[9] S. Wang, Y. Jiang, E. J. Juarez-Perez, L. K. Ono, Y. Qi, *Nat. Energy* **2016**, *2*, 16195.
[10] F. Fu, S. Pisoni, Q. Jeangros, J. Sastre-Pellicer, M. Kawecki, A. Paracchino, T. Moser, J. Werner, C. Andres, L. Duchêne, P. Fiala, M. Rawlence, S. Nicolay, C. Ballif, A. N. Tiwari, S. Buecheler, *Energy Environ. Sci.* **2019**, *12*, 3074.
[11] J. L. Minns, P. Zajdel, D. Chernyshov, W. van Beek, M. A. Green, *Nat. Commun.* **2017**, *8*, 15152.
[12] C. Li, A. Guerrero, S. Huettner, J. Bisquert, *Nat. Commun.* **2018**, *9*, 5113.
[13] D. Meggiolaro, S. G. Motti, E. Mosconi, A. J. Barker, J. Ball, C. A. R. Perini, F. Deschler, A. Petrozza, F. De Angelis, *Energy Environ. Sci.* **2018**, *11*, 702.
[14] W. Li, J. Liu, F. Q. Bai, H. X. Zhang, O. V. Prezhdo, *ACS Energy Lett.* **2017**, *2*, 1270.
[15] W. D. Tang, T. J. Liu, M. Y. Zhang, F. L. Yuan, K. Zhou, R. C. Lai, Y. X. Lian, S. Y. Xing, W. T. Xiong, M. Zhang, F. Gao, B. D. Zhao, D. W. Di, *Matter* **2023**, *6*, 3782.
[16] G. Tumen-Ulzii, C. J. Qin, T. Matsushima, M. R. Leyden, U. Balijipalli, D. Klotz, C. Adachi, *Sol. RRL* **2020**, *4*, 2000305.
[17] R. A. Kerner, L. F. Zhao, S. P. Harvey, J. J. Berry, J. Schwartz, B. P. Rand, *ACS Energy Lett.* **2020**, *5*, 3352.
[18] Z. Xu, D. D. Astridge, R. A. Kerner, X. Zhong, J. Hu, J. Hong, J. A. Wisch, K. Zhu, J. J. Berry, A. Kahn, A. Sellinger, B. P. Rand, *J. Am. Chem. Soc.* **2023**, *145*, 11846.
[19] Y. Yang, S. Cheng, X. Zhu, S. Li, Z. Zheng, K. Zhao, L. Ji, R. Li, Y. Liu, C. Liu, Q. Lin, N. Yan, Z. Wang, *Nat. Energy* **2023**, *9*, 37.
[20] K. Schutt, P. K. Nayak, A. J. Ramadan, B. Wenger, Y. H. Lin, H. J. Snaith, *Adv. Funct. Mater.* **2019**, *29*, 1900466.
[21] M. Wang, Z. Shi, C. Fei, Z. J. D. Deng, G. Yang, S. P. Dunfield, D. P. Fenning, J. Huang, *Nat. Energy* **2023**, *8*, 1229.
[22] J. Liang, A. Sun, Z. Zhang, Y. Zheng, X. Wu, C. Tian, Z. Chen, C.-C. Chen, *ACS Mater. Lett.* **2023**, *5*, 1395.
[23] R. A. Kerner, T. H. Schloemer, P. Schulz, J. J. Berry, J. Schwartz, A. Sellinger, B. P. Rand, *J. Mater. Chem. C* **2019**, *7*, 5251.
[24] R. A. Kerner, T. H. Schloemer, P. Schulz, J. J. Berry, J. Schwartz, A. Sellinger, B. P. Rand, *J. Mater. Chem. C* **2019**, *7*, 5244.
[25] J. N. Hu, R. A. Kerner, I. Pelczer, B. P. Rand, J. Schwartz, *ACS Energy Lett.* **2021**, *6*, 2262.
[26] K. Domanski, E. A. Alharbi, A. Hagfeldt, M. Grätzel, W. Tress, *Nat. Energy* **2018**, *3*, 61.
[27] M. Khenkin, H. Köbler, M. Remec, R. Roy, U. Erdil, J. Li, N. Phung, G. Adwan, G. Paramasivam, Q. Emery, E. Unger, R. Schlatmann, C. Ulbrich, A. Abate, *Energy Environ. Sci.* **2024**, *17*, 602.
[28] M. V. Khenkin, E. A. Katz, A. Abate, G. Bardizza, J. J. Berry, C. Brabec, F. Brunetti, V. Bulovic, Q. Burlingame, A. Di Carlo, R. Cheacharoen, Y. B. Cheng, A. Colsmann, S. Cros, K. Domanski, M. Dusza, C. J. Fell, S. R. Forrest, Y. Galagan, D. Di Girolamo, M. Graetzel, A. Hagfeldt, E. von Hauff, H. Hoppe, J. Kettle, H. Koebler, M. S. Leite, S. Liu, Y. L. Loo, J. M. Luther, et al., *Nat. Energy* **2020**, *5*, 35.
[29] P. Chen, Y. Xiao, J. Hu, S. Li, D. Luo, R. Su, P. Caprioglio, P. Kaienburg, X. Jia, N. Chen, J. Wu, Y. Sui, P. Tang, H. Yan, T. Huang, M. Yu, Q. Li, L. Zhao, C. H. Hou, Y. W. You, J. J. Shyue, D. Wang, X. Li, Q. Zhao, Q. Gong, Z. H. Lu, H. J. Snaith, R. Zhu, *Nature* **2024**, *625*, 516.
[30] S. Sidhik, I. Metcalf, W. Li, T. Kodalle, C. J. Dolan, M. Khalili, J. Hou, F. Mandani, A. Torma, H. Zhang, R. Garai, J. Persaud, A. Marciel, I. A. Muro Puente, G. N. M. Reddy, A. Balvanz, M. A. Alam, C. Katan, E. Tsai, D. Ginger, D. P. Fenning, M. G. Kanatzidis, C. M. Sutter-Fella, J. Even, A. D. Mohite, *Science* **2024**, *384*, 1227.
[31] W. T. Wang, P. Holzhey, N. Zhou, Q. Zhang, S. Zhou, E. A. Duijnstee, K. J. Rietwyk, J. Y. Lin, Y. Mu, Zhang, U. Bach, C. G. Wu, H. L. Yip, H. J. Snaith, S. P. Feng, *Nature* **2024**, *632*, 294.
[32] C. Liu, Y. Yang, H. Chen, I. Spanopoulos, A. S. R. Bati, I. W. Gilley, J. Chen, A. Maxwell, B. Vishal, R. P. Reynolds, T. E. Wiggins, Z. Wang, C. Huang, J. Fletcher, Y. Liu, L. X. Chen, S. De Wolf, B. Chen, D. Zheng, T. J. Marks, A. Facchetti, E. H. Sargent, M. G. Kanatzidis, *Nature* **2024**, *633*, 359.
[33] J. Luo, B. Liu, H. Yin, X. Zhou, M. Wu, H. Shi, J. Zhang, J. Elia, K. Zhang, J. Wu, Z. Xie, C. Liu, J. Yuan, Z. Wan, T. Heumueller, L. Luer, E. Spiecker, N. Li, C. Jia, C. J. Brabec, Y. Zhao, *Nat. Commun.* **2024**, *15*, 2002.
[34] Q. Li, Y. Zheng, H. Wang, X. Liu, M. Lin, X. Sui, X. Leng, D. Liu, Z. Wei, M. Song, D. Li, H. G. Yang, S. Yang, Y. Hou, *Science* **2025**, *387*, 1069.
[35] S. Tan, M. C. Shih, Y. Lu, S. G. Choi, Y. Dong, J. H. Lee, I. Yavuz, B. W. Larson, S. Y. Park, T. Kodalle, R. Zhang, M. J. Grotevent, Y. K. Lin, H. Zhu, V. Bulovic, C. M. Sutter-Fella, N. G. Park, M. C. Beard, J. W. Lee, K. Zhu, M. G. Bawendi, *Science* **2025**, *388*, 639.
[36] H. Zai, P. Yang, J. Su, R. Yin, R. Fan, Y. Wu, X. Zhu, Y. Ma, T. Zhou, W. Zhou, Y. Zhang, Z. Huang, Y. Jiang, N. Li, Y. Bai, C. Zhu, Z. Huang, J. Chang, Q. Chen, Y. Zhang, H. Zhou, *Science* **2025**, *387*, 186.
[37] S. You, H. Zhu, Z. Shen, X. Wang, B. Shao, Q. Wang, J. Lu, Y. Yuan, B. D. Dou, E. M. Sanehira, T. Russell, A. Lorenz, Y. Dong, L. Chen, M. Casareto, N. Rolston, M. C. Beard, J. J. Berry, M. Freitag, Y. Yan, O. M. Bakr, K. Zhu, *Science* **2025**, *388*, 964.
[38] J. H. Heo, S. Y. Hong, J. K. Park, H. J. Lee, F. Zhang, S. H. Im, *Joule* **2025**, *9*, 101850.
[39] Y. H. Lin, N. Sakai, P. Da, J. Wu, H. C. Sansom, A. J. Ramadan, S. Mahesh, J. Liu, R. D. J. Oliver, J. Lim, L. Aspitarte, K. Sharma, P. K. Madhu, A. B. Morales-Vilches, P. K. Nayak, S. Bai, F. Gao, C. R. M. Grovenor, M. B. Johnston, J. G. Labram, J. R. Durrant, J. M. Ball, B. Wenger, B. Stannowski, H. J. Snaith, *Science* **2020**, *369*, 96.
[40] Y. Zhao, T. Heumueller, J. Zhang, J. Luo, O. Kasian, S. Langner, C. Kupfer, B. Liu, Y. Zhong, J. Elia, A. Osvet, J. Wu, C. Liu, Z. Wan, C. Jia, N. Li, J. Hauch, C. J. Brabec, *Nat. Energy* **2021**, *7*, 144.

[41] V. Paraskeva, M. Hadjipanayi, M. Norton, A. Aguirre, A. Hadipour, R. Ebner, G. E. Georghiou, in 2022 IEEE 49th Photovoltaics Specialists Conference (PVSC), IEEE, Philadelphia, PA, USA **2022**, p. 0217.
[42] V. Paraskeva, M. Hadjipanayi, M. Norton, A. Aguirre, A. Hadipour, W. Y. Song, T. Fontanot, S. Christiansen, R. Ebner, G. E. Georghiou, *Energies* **2023**, *16*, 2608.
[43] Y. Zhang, Y. Chen, G. Liu, Y. Wu, Z. Guo, R. Fan, K. Li, H. Liu, Y. Zhao, T. Kodalle, Y. Chen, C. Zhu, Y. Bai, Q. Chen, H. Zhou, *Science* **2025**, *387*, 284.
[44] Y. X. Guo, C. Zhang, L. Q. Wang, X. T. Yin, B. H. Sun, C. T. Wei, X. Luo, S. Y. Yang, L. C. Sun, B. Xu, *Energy Environ. Sci.* **2025**, *18*, 2308.
[45] Z. Peng, A. Vincze, F. Streller, V. M. Le Corre, K. C. Zhang, C. H. Li, J. J. Tian, C. Liu, J. S. Luo, Y. C. Zhao, A. Späth, R. Fink, T. Heumüller, A. Osvet, N. Li, M. Stolterfoht, L. Lüer, C. J. Brabec, *Energy Environ. Sci.* **2024**, *17*, 8313.
[46] A. Julien, J.-B. Puel, J.-F. Guillemoles, *Energy Environ. Sci.* **2023**, *16*, 190.
[47] C. Liu, L. Luer, V. M. L. Corre, K. Forberich, P. Weitz, T. Heumuller, X. Du, J. Wortmann, J. Zhang, J. Wagner, L. Ying, J. Hauch, N. Li, C. J. Brabec, *Adv. Mater.* **2024**, *36*, 2300259.
[48] A. Levtchenko, A. Julien, D. McDermott, J. B. Puel, J. F. Guillemoles, D. Ory, D. Suchet, *Sol. RRL* **2024**, *8*, 2400511.
[49] A. Dasgupta, S. Mahesh, P. Caprioglio, Y. H. Lin, K. A. Zaininger, R. D. J. Oliver, P. Holzhey, S. Zhou, M. M. McCarthy, J. A. Smith, M. Frenzel, M. G. Christoforo, J. M. Ball, B. Wenger, H. J. Snaith, *ACS Energy Lett.* **2022**, *7*, 2311.
[50] A. D. Bui, D. T. Nguyen, A. Fell, N. Mozaffari, V. Ahmad, T. Duong, L. Li, T. N. Truong, A. A. Wibowo, K. Nguyen, O. Fischer, F. Schindler, M. C. Schubert, K. J. Weber, T. P. White, K. R. Catchpole, D. Macdonald, H. T. Nguyen, *Cell Rep. Phys. Sci.* **2023**, *4*, 101641.
[51] F. Lang, E. Köhnen, J. Warby, K. Xu, M. Grischek, P. Wagner, D. Neher, L. Korte, S. Albrecht, M. Stolterfoht, *ACS Energy Lett.* **2021**, *6*, 3982.
[52] M. Stolterfoht, C. M. Wolff, J. A. Márquez, S. S. Zhang, C. J. Hages, D. Rothhardt, S. Albrecht, P. L. Burn, P. Meredith, T. Unold, D. Neher, *Nat. Energy* **2018**, *3*, 847.
[53] A. D. Bui, M. A. Mahmud, N. Mozaffari, R. Basnet, T. Duong, G. Bartholazzi, T. T. Le, T. N. Truong, M. Tebyetekerwa, A. Wibowo, K. J. Weber, T. P. White, K. R. Catchpole, D. Macdonald, H. T. Nguyen, *Sol. RRL* **2021**, *5*, 2100348.
[54] L. Wagner, P. Schygulla, J. P. Herterich, M. Elshamy, D. Bogachuk, S. Zouhair, S. Mastroianni, U. Wuerfel, Y. H. Liu, S. M. Zakeeruddin, M. Graetzel, A. Hinsch, S. W. Glunz, *Matter* **2022**, *5*, 2352.
[55] J. J. van Franeker, K. H. Hendriks, B. J. Bruijnaers, M. W. G. M. Verhoeven, M. M. Wienk, R. A. J. Janssen, *Adv. Energy Mater.* **2016**, *7*, 201601822.
[56] A. F. V. Fonseca, L. Scalon, B. R. C. Vale, M. G. D. Guaita, J. Bettini, Z. C. Brandao, L. F. Zagonel, L. A. Padilha, A. F. Nogueira, *ACS Energy Lett.* **2024**, *9*, 3177.
[57] J. Warby, S. H. Shah, J. Thiesbrummel, E. Gutierrez-Partida, H. G. Lai, B. Alebachew, M. Grischek, F. J. Yang, F. L. Lang, S. Albrecht, F. Fu, D. Neher, M. Stolterfoht, *Adv. Energy Mater.* **2023**, *13*, 2303135.
[58] P. Caprioglio, M. Stolterfoht, C. M. Wolff, T. Unold, B. Rech, S. Albrecht, D. Neher, *Adv. Energy Mater.* **2019**, *9*, 1901631.
[59] M. Koopmans, V. Corre, L. Koster, *J. Open Source Softw.* **2022**, *7*, 3727.
[60] A. These, L. J. A. Koster, C. J. Brabec, V. M. Le Corre, *Adv. Energy Mater.* **2024**, *14*, 2400055.
[61] W. D. Xu, L. J. F. Hart, B. Moss, P. Caprioglio, T. J. Macdonald, F. Furlan, J. Panidi, R. D. J. Oliver, R. A. Pacalaj, M. Heeney, N. Gasparini, H. J. Snaith, P. R. F. Barnes, J. R. Durrant, *Adv. Energy Mater.* **2023**, *13*, 2301102.
[62] J. Herterich, M. Unmüssig, G. Loukeris, M. Kohlstädt, U. Würfel, *Energy Technol.* **2021**, *9*, 2001104.
[63] F. Fiorentino, M. D. Albaqami, I. Poli, A. Petrozza, *ACS Appl. Mater. Interfaces* **2022**, *14*, 34180.
[64] C. L. Zhang, S. H. Wu, L. M. Tao, G. M. Arumugam, C. Liu, Z. Wang, S. S. Zhu, Y. Z. Yang, J. Lin, X. Y. Liu, R. E. I. Schropp, Y. H. Mai, *Adv. Energy Mater.* **2020**, *10*, 2002004.
[65] A. A. Sutanto, R. Szostak, N. Drigo, V. I. E. Queloz, P. E. Marchezi, J. C. Germino, H. C. N. Tolentino, M. K. Nazeeruddin, A. F. Nogueira, G. Grancini, *Nano Lett.* **2020**, *20*, 3992.
[66] C. A. R. Perini, E. Rojas-Gatjens, M. Ravello, A. F. Castro-Mendez, J. Hidalgo, Y. An, S. Kim, B. Lai, R. Li, C. Silva-Acuna, J. P. Correa-Baena, *Adv. Mater.* **2022**, *34*, 2204726.
[67] H. Chen, S. Teale, B. Chen, Y. Hou, L. Grater, T. Zhu, K. Bertens, S. M. Park, H. R. Atapattu, Y. J. Gao, M. Y. Wei, A. K. Johnston, Q. L. Zhou, K. M. Xu, D. N. Yu, C. C. Han, T. Cui, E. H. Jung, C. Zhou, W. J. Zhou, A. H. Proppe, S. Hoogland, F. Laquai, T. Filleter, K. R. Graham, Z. J. Ning, E. H. Sargent, *Nat. Photonics* **2022**, *16*, 352.
[68] Akriti, S. Zhang, Z. Y. Lin, E. Shi, B. P. Finkenauer, Y. Gao, A. J. Pistone, K. Ma, B. M. Savoie, L. Dou, *Adv. Mater.* **2021**, *33*, 2105183.
[69] J. H. Liang, Z. F. Zhang, Y. Huang, Q. Xue, Y. T. Zheng, X. Y. Wu, C. C. Tian, Y. Zhang, Y. M. Wang, Z. H. Chen, C. C. Chen, *Adv. Funct. Mater.* **2022**, *32*, 2207177.
[70] S. You, H. Zeng, Y. Liu, B. Han, M. Li, L. Li, X. Zheng, R. Guo, L. Luo, Z. Li, C. Zhang, R. Liu, Y. Zhao, S. Zhang, Q. Peng, T. Wang, Q. Chen, F. T. Eickemeyer, B. Carlsen, S. M. Zakeeruddin, L. Mai, Y. Rong, M. Gratzel, X. Li, *Science* **2023**, *379*, 288.
[71] R. A. Kerner, S. Heo, K. Roh, K. MacMillan, B. W. Larson, B. P. Rand, *ACS Energy Lett.* **2021**, *6*, 501.
[72] J. Hong, Z. Xu, D. Lungwitz, J. Scott, H. M. Johnson, Y.-H. Kim, A. Kahn, B. P. Rand, *ACS Energy Lett.* **2023**, *8*, 4984.
[73] X. Zhao, T. Liu, Q. C. Burlingame, T. Liu, R. Holley, 3rd, G. Cheng, N. Yao, F. Gao, Y. L. Loo, *Science* **2022**, *377*, 307.
[74] Z. Dai, S. K. Yadavalli, M. Chen, A. Abbaspourtamijani, Y. Qi, N. P. Padture, *Science* **2021**, *372*, 618.
[75] H. Tang, Z. Shen, Y. Shen, G. Yan, Y. Wang, Q. Han, L. Han, *Science* **2024**, *383*, 1236.
[76] M. A. Truong, T. Funasaki, L. Ueberricke, W. Nojo, R. Murdey, T. Yamada, S. Hu, A. Akatsuka, N. Sekiguchi, S. Hira, L. Xie, T. Nakamura, N. Shioya, D. Kan, Y. Tsuji, S. Iikubo, H. Yoshida, Y. Shimakawa, T. Hasegawa, Y. Kanemitsu, T. Suzuki, A. Wakamiya, *J. Am. Chem. Soc.* **2023**, *145*, 7528.
[77] E. P. Li, C. Liu, H. Z. Lin, X. J. Xu, S. J. Liu, S. Zhang, M. J. Yu, X. M. Cao, Y. Z. Wu, W. H. Zhu, *Adv. Funct. Mater.* **2021**, *31*, 2103847.
[78] K. Zhao, Q. Liu, L. Yao, C. Deger, J. Shen, X. Zhang, P. Shi, Y. Tian, Y. Luo, J. Xu, J. Zhou, D. Jin, S. Wang, W. Fan, S. Zhang, S. Chu, X. Wang, L. Tian, R. Liu, L. Zhang, I. Yavuz, H. F. Wang, D. Yang, R. Wang, J. Xue, *Nature* **2024**, *632*, 301.
[79] M. Liu, M. L. Li, Y. X. Li, Y. D. An, Z. F. Yao, B. B. Fan, F. Qi, K. K. Liu, H. L. Yip, F. R. Lin, A. K. Y. Jen, *Adv. Energy Mater.* **2024**, *14*, 2303742.
[80] Z. H. Dai, S. You, D. Chakraborty, S. R. Li, Y. D. Zhang, A. Ranka, S. Barlow, J. J. Berry, S. R. Marder, P. J. Guo, Y. Qi, K. Zhu, N. P. Padture, *ACS Energy Lett.* **2024**, *9*, 1880.
[81] I. Levine, A. Al-Ashouri, A. Musiienko, H. Hempel, A. Magomedov, A. Drevilkauskaite, V. Getautis, D. Menzel, K. Hinrichs, T. Unold, S. Albrecht, T. Dittrich, *Joule* **2021**, *5*, 2915.
[82] L. V. Torres Merino, C. E. Petoukhoff, O. Matiash, A. S. Subbiah, C. V. Franco, P. Dally, B. Vishal, S. Kosar, D. Rosas Villalva, V. Hnapovskyi, E. Ugur, S. Shah, F. Peña Camargo, O. Karalis, H. Hempel, I. Levine, R. R. Pradhan, S. Kralj, N. Kalasariya, M. Babics, B. K. Yildirim, A. A. Said, E. Aydin, H. Bristow, S. Mannar, W. Raja, A. R. Pininti, A. Prasetio, A. Razzaq, et al., *Joule* **2024**, *8*, 2585.
[83] R. A. Kerner, Z. J. Xu, B. W. Larson, B. P. Rand, *Joule* **2021**, *5*, 2273.
[84] S. R. Lee, D. Lee, S. G. Choi, S. K. Jung, J. H. Lee, M. c. Kim, J. S. Park, J. W. Lee, *Sol. RRL* **2024**, *8*, 2300958.

[85] J. X. Xia, Y. Zhang, C. X. Xiao, K. G. Brooks, M. Chen, J. S. Luo, H. Yang, N. I. D. Klipfel, J. H. Zou, Y. Shi, X. J. Yao, J. Z. Chen, J. M. Luther, H. Z. Lin, A. M. Asiri, C. Y. Jia, M. K. Nazeeruddin, *Joule* **2022**, *6*, 1689.
[86] X. Wu, B. Li, Z. Zhu, C. C. Chueh, A. K. Jen, *Chem. Soc. Rev.* **2021**, *50*, 13090.
[87] H.-R. Bai, Q. An, H.-F. Zhi, M. Jiang, A. Mahmood, L. Yan, M.-Q. Liu, Y.-Q. Liu, Y. Wang, J.-L. Wang, *ACS Energy Lett.* **2022**, *7*, 3045.
[88] R. Ma, T. Liu, Z. Luo, Q. Guo, Y. Xiao, Y. Chen, X. Li, S. Luo, X. Lu, M. Zhang, Y. Li, H. Yan, *Sci. China: Chem.* **2020**, *63*, 325.
[89] A. P. Zeng, X. L. Ma, M. G. Pan, Y. Z. Chen, R. J. Ma, H. Zhao, J. Q. Zhang, H. Kim, A. Shang, S. W. Luo, I. C. Angunawela, Y. Chang, Z. Y. Qi, H. L. Sun, J. Y. L. Lai, H. Ade, W. Ma, F. J. Zhang, H. Yan, *Adv. Funct. Mater.* **2021**, *31*, 2102413.
[90] A. K. Jena, A. Kulkarni, T. Miyasaka, *Chem. Rev.* **2019**, *119*, 3036.
[91] J. H. Tao, C. H. Zhao, Z. J. Wang, Y. Chen, L. L. Zang, G. Yang, Y. Bai, J. H. Chu, *Energy Environ. Sci.* **2025**, *18*, 509.
[92] Y. Lin, B. Chen, Y. Fang, J. Zhao, C. Bao, Z. Yu, Y. Deng, P. N. Rudd, Y. Yan, Y. Yuan, J. Huang, *Nat. Commun.* **2018**, *9*, 4981.
[93] S. Ravishankar, O. Almora, C. Echeverria-Arrondo, E. Ghahremanirad, C. Aranda, A. Guerrero, F. Fabregat-Santiago, A. Zaban, G. Garcia-Belmonte, J. Bisquert, *J. Phys. Chem. Lett.* **2017**, *8*, 915.
[94] Q. Wang, *J. Phys. Chem. C* **2018**, *122*, 4822.
[95] Z. Peng, J. Tian, K. Zhang, A. These, Z. Xie, Y. Zhao, A. Osvet, F. Guo, L. Lüer, N. Li, C. J. Brabec, *ACS Energy Lett.* **2023**, *8*, 2077.
[96] E. J. Juarez-Perez, L. K. Ono, M. Maeda, Y. Jiang, Z. Hawash, Y. B. Qi, *J. Mater. Chem. A* **2018**, *6*, 9604.
[97] L. Ma, D. Guo, M. Li, C. Wang, Z. Zhou, X. Zhao, F. Zhang, Z. Ao, Z. Nie, *Chem. Mat.* **2019**, *31*, 8515.
[98] J. Hu, J. W. Ahn, Z. Xu, M. J. Jeong, C. Kim, J. H. Noh, H. Min, B. P. Rand, *Adv. Energy Mater.* **2024**, *14*, 2400500.
[99] J. Park, J. Kim, H. S. Yun, M. J. Paik, E. Noh, H. J. Mun, M. G. Kim, T. J. Shin, S. I. Seok, *Nature* **2023**, *616*, 724.
[100] S. Qiu, L. Dong, D. Jang, F. Yang, J. G. Cerrillo, C. Li, Z. Xie, J. Luo, F. Guo, A. Distler, T. Du, C. J. Brabec, H. J. Egelhaaf, *Adv. Energy Mater.* **2024**, *14*, 2402616.
[101] J. S. Cho, P. V. Kamat, *Chem. Mat.* **2020**, *32*, 6206.
[102] M. I. Saidaminov, J. Kim, A. Jain, R. Quintero-Bermudez, H. R. Tan, G. K. Long, F. R. Tan, A. Johnston, Y. C. Zhao, O. Voznyy, E. H. Sargent, *Nat. Energy* **2018**, *3*, 648.
[103] M. Bag, L. A. Renna, R. Y. Adhikari, S. Karak, F. Liu, P. M. Lahti, T. P. Russell, M. T. Tuominen, D. Venkataraman, *J. Am. Chem. Soc.* **2015**, *137*, 13130.
[104] J. Haruyama, K. Sodeyama, L. Han, Y. Tateyama, *J. Am. Chem. Soc.* **2015**, *137*, 10048.
[105] X. Gao, Y. Zhang, T. Zhang, Y. Wu, Q. Ji, M. G. Ju, J. Wang, *J. Phys. Chem. Lett.* **2024**, *15*, 5779.